Pack aluminisation kinetics of nickel rods and foams

D. C. Dunand, A. M. Hodge & C. Schuh

Pack aluminisation kinetics of nickel rods and foams

D. C. Dunand, A. M. Hodge, and C. Schuh

The kinetics of pack aluminisation has been described through a multiphase, finite difference model considering diffusion of aluminium into nickel under conditions of concentration dependent diffusivity and finite specimen dimensions, allowing complete conversion of the specimen to the equilibrium intermetallic phase. For a cylindrical geometry, the model accurately predicts the growth of an outer Ni_2Al_3 shell, the increase in diameter, and the average composition as measured for 0·5 and 1 mm diameter nickel rods aluminised at 1000°C for up to 4 h. For nickel foams with hollow struts, which are modelled as thin sheets, good agreement is found with the average aluminium concentration measured on two foams with strut wall thicknesses of 41 and 84 νm. The measured aluminisation kinetics for a foam with strut thickness of 6 νm, however, is much slower than predicted owing to the high surface area of this foam, which prevents the centre of the specimen from reaching the equilibrium aluminium surface concentration.   MST/5093

The authors are in the Department of Materials Science and Engineering, Northwestern University, Evanston, IL 60208, USA. (dunand@northwestern.edu) Manuscript received 8 May 2001; accepted 17 May 2001.

Introduction

Metallic foams, with uses in acoustic, thermal, or structural applications,[1] exhibit strength, stiffness, and temperature- and environment resistance that are much higher than those of polymer foams, but lower than those of ceramic foams. A possible improvement in the last two properties, while conserving the excellent toughness, ductility, and thermal and electrical conductivity of metals, can be achieved through the development of intermetallic compound foams. Because of the high melting point, excellent oxidation resistance, and good high temperature mechanical properties of nickel aluminides (NiAl or Ni_3Al),[2–4] foams based on these intermetallics are promising for aerospace applications.[5] However, these foams are difficult to produce by traditional liquid phase methods, because of the high melting temperatures and high reactivity of NiAl or Ni_3Al melts.

In previous work,[5] it was demonstrated experimentally that nickel aluminide foams could be produced by diffusion of aluminium deposited from the gas phase onto the surface of a nickel foam. This pack aluminisation technique is well established for creating protective NiAl or Ni_3Al coatings on nickel and nickel based superalloy parts that are much thicker than the coating, and the kinetics of this process has been extensively studied.[6–9] In contrast, the previous work[5] demonstrated that open cell nickel foams could be completely converted to nickel aluminide at 1000°C in a few hours by a two step pack aluminisation, owing to the small diffusion distances in the foam struts. The goal of the present study was to carry out a diffusion analysis of this conversion process, and to compare its predictions with experimental results published previously[5] as well as new experimental results for foam aluminisation. The model allows for quantitative prediction of the pack aluminisation process parameters (temperature, time, and gas composition) to achieve a given average aluminium composition (and thus aluminide phase), starting from an initial nickel foam with known wall thickness.

Experimental procedures

Three unalloyed nickel foams (>99·0% purity) were studied: two coarse cell foams with 20 and 30 pores/linear inch (ppi), respectively, from Astro Met (Cincinnati, OH, USA), and one fine cell foam with 80 pores/linear inch from Goodfellow (Cambridge, UK). As summarised in Table 1, the foams exhibited various relative densities (ratio of foam density/solid density, obtained from mass and volume measurements) and geometric parameters (cell size, strut width, and strut wall thickness, measured using scanning electron micrographs).

Aluminisation was carried out under argon at 1000°C, using a high activity powder pack consisting of 3 wt-% ammonium chloride, 15 wt-% aluminium, and 82 wt-% alumina. Further experimental details can be found elsewhere.[5] To assess aluminisation kinetics for more simple geometries, aluminisation experiments were also conducted on thin nickel rods (99·99% purity, from Alfa Aesar, Ward Hill, MA, USA) with diameters of 0·5 and 1·0 mm, and lengths ranging from 32 to 39 mm. Average specimen compositions were determined through mass gain measurements by weighing foams before and after aluminisation; the accuracy of this technique was checked by wet chemical analysis. Composition errors of ±1 wt-% were estimated from the two main sources of error affecting the aluminised

Table 1 Geometric parameters of nickel foams

Pores/linear inch (ppi)*	Foam thickness, mm	Cell diameter†, mm	Strut width, μm	Strut wall thickness, μm	Relative density, %
20	8·7	1·27	224±34	83·5±21·3	2·2
30	4·1–7·0	0·85	117±21	40·5±6·5	3·0
80	1·6	0·32	54·9±5·0	6·0±1·1	3·5

*Data from supplier.
†Calculated from ppi value.
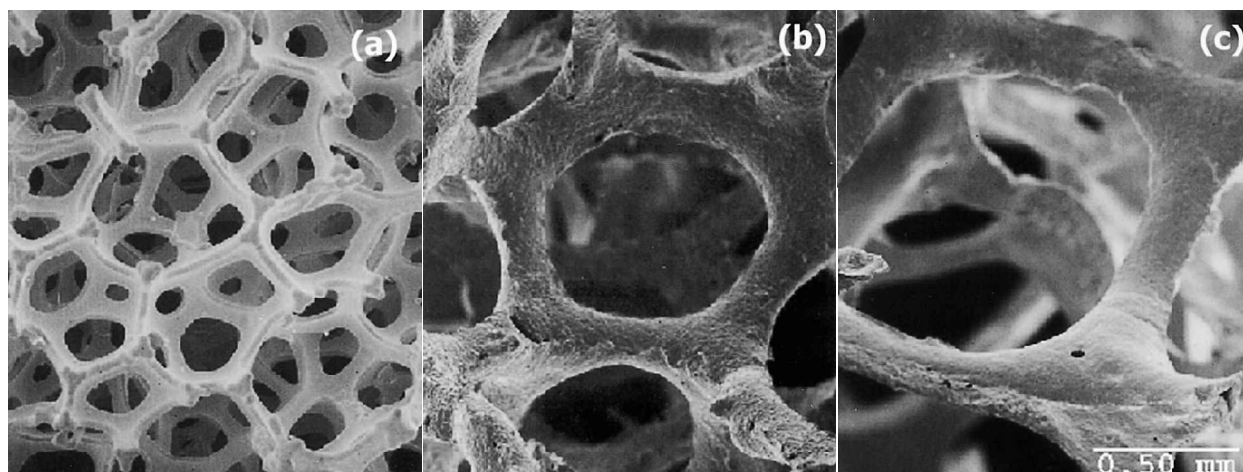
a 80 ppi; b 30 ppi; c 20 ppi

1   Images (SEM) of as received nickel foams with given cell sizes

foam mass measurement, i.e. small losses of the brittle foam material during manipulation and ultrasonic cleaning, and small additions of alumina powders not detached from the foam during cleaning. For rods, the diameter was also measured using calipers before and after aluminisation.

Metallographic preparation of foam and rod specimens was carried out using standard techniques, and phases were identified by optical observation, Vickers microhardness measurements (100 g load for 15 s), or energy dispersive spectroscopy (EDS) in a scanning electron microscope (SEM).

## Experimental results

PHASES

The as received nickel foams are shown in Fig. 1, which illustrates the varying cell size, strut width and strut wall thickness (given in Table 1), the last representing the diffusion distance over which aluminisation takes place. After aluminisation, the foams conserved the same overall geometry (open cells and hollow struts) and macroscopic size and shape.[5] When the foams were cut into halves, a macroscopic gradient of composition was visible in terms of

a change of colour, indicative of an inner, nickel rich and an outer, aluminium rich region in the foams.[10] Mass measurements on 80 pores/linear inch (ppi) foams aluminised to full saturation for 4 h or more yielded an average composition of 59·6 at.-%Al, corresponding to the Ni_2Al_3 phase. This composition represents the equilibrium aluminium surface concentration established during aluminisation, which is thermodynamically fixed by the pack composition and temperature.[9,11]

A metallographic section of an aluminised 30 ppi foam is shown in Fig. 2 (micrographs for 20 and 80 ppi foams reported elswhere[5] are qualitatively similar). It can be seen that three walls enclose the internal cavity of a hollow strut (triangular black area). The thinnest wall is single phase Ni_2Al_3, while the other, thicker walls exhibit multiple phases consisting of: a thick, outer Ni_2Al_3 surface layer (denoted by 1 in Fig. 2); a thinner, intermediate $NiAl-Ni_3Al$ layer (2) and a central nickel region (3). The same layer sequence is visible from the inner wall surface, illustrating that aluminisation occurred from both the inner and the outer surfaces of the hollow struts. However, the inner Ni_2Al_3 layer is noticeably thinner than the outer one, indicating that the aluminium flux was larger on the outer strut surface. The plane of polishing is most probably not perpendicular to the two thicker walls, leading to apparent wall and layer dimensions larger than their nominal values.
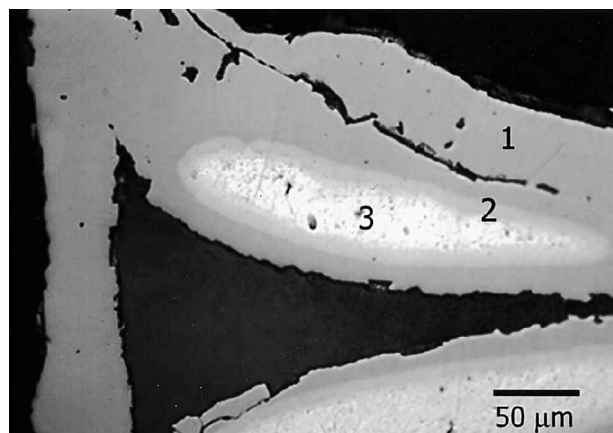
2   Optical micrograph of metallographic section of 30 ppi foam aluminised for 1 h, showing triangular strut: labelled on one strut wall are outer Ni_2Al_3 layer (1), intermediate $NiAl-Ni_3Al$ layer (2), and central Ni region (3); crack in Ni_2Al_3 layer is due to metallographic preparation
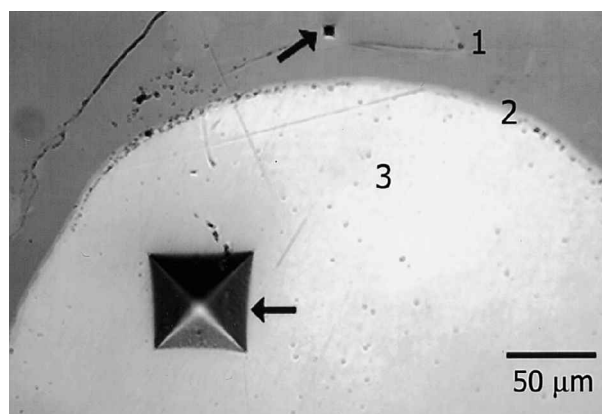
3   Metallographic cross-section of 0·5 mm rod aluminised for 4 h: outer Ni_2Al_3 shell (1) is in contact with thin $NiAl-Ni_3Al$ ring (2) also exhibiting some Kirkendall porosity, which surrounds unreacted Ni region (3) in centre of rod; two Vickers indents are marked by arrows
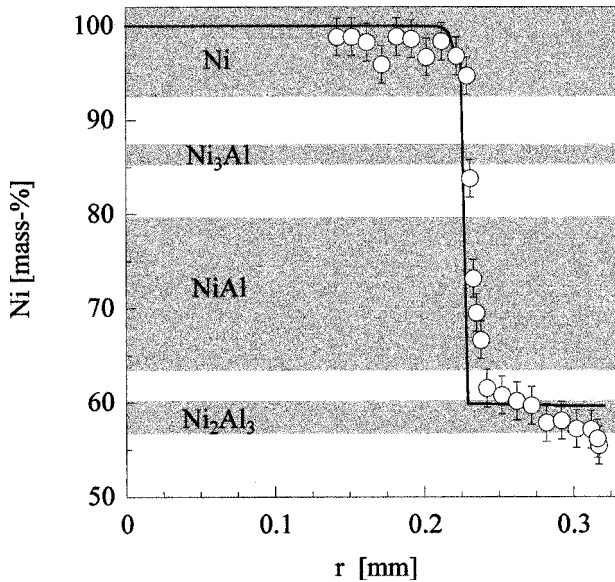
4 Measured composition as function of distance r from centre of 0·5 mm rod aluminised for 4 h: curve is predicted composition profile and phase composition ranges at 1000°C (Ref. 11) are shown as shaded bands

The larger size and simpler geometry of the aluminised rods allowed a clearer illustration of the above results, as seen in Fig. 3, showing a cross-section of a 0·5 mm diameter rod aluminised for 4 h. The rod exhibits a thick, outer Ni_2Al_3 shell (1) in contact with a very thin $NiAl - Ni_3Al$ ring ~ 3 μm in width (2) surrounding an untransformed nickel core (3). In Fig. 3, two Vickers indents (marked by arrows) illustrate the much higher hardness of the Ni_2Al_3 phase, compared with nickel. The hardness of NiAl is intermediate between those of the above two phases, so indents are a rapid and convenient means of identifying phases. A concentration gradient, as measured by EDS on the same specimen, is shown in Fig. 4, and exhibits the expected discontinuity when the phase boundaries are crossed.

ALUMINISATION KINETICS

Figure 5a shows the thickness of the Ni_2Al_3 shell as a function of aluminising time for the two rods, which seems to increase somewhat more rapidly for the 0·5 mm rod. As expected for a diffusion controlled process, the penetration rate of the shell diminishes monotonically with time. In Fig. 5b, the rod diameter increase is plotted as a function of aluminising time, and shows the same monotonic trend as in Fig. 5a; within error, the two rods exhibit the same amount of swelling. Finally, Fig. 6 shows the aluminium mass gain (expressed as average nickel concentration) as a function of aluminisation time for the two rods. While the thicker, 1 mm rods did not reach the Ni_3Al composition after 4 h., the thinner 0·5 mm rods displayed an average Ni_3Al composition after 2 h, and $NiAl - Ni_3Al$ composition after 4 h of aluminisation.

Figure 7 provides aluminisation kinetics data for the three foams studied, which, as expected, exhibit faster aluminisation with increasing surface/volume ratio or, equivalently, decreasing diffusion depth. The Ni_3Al composition was reached after ~ 1·5, 0·5, and 0·2 h for the 20, 30, and 80 ppi foams, with respective average wall thicknesses of 84, 41, and 6 μm. Stoichiometric NiAl composition was not reached by the 20 ppi foam after the maximum experimental aluminisation time of 4 h, and required ~ 3 and 1·5 h for the 30 and 80 ppi foams, respectively.
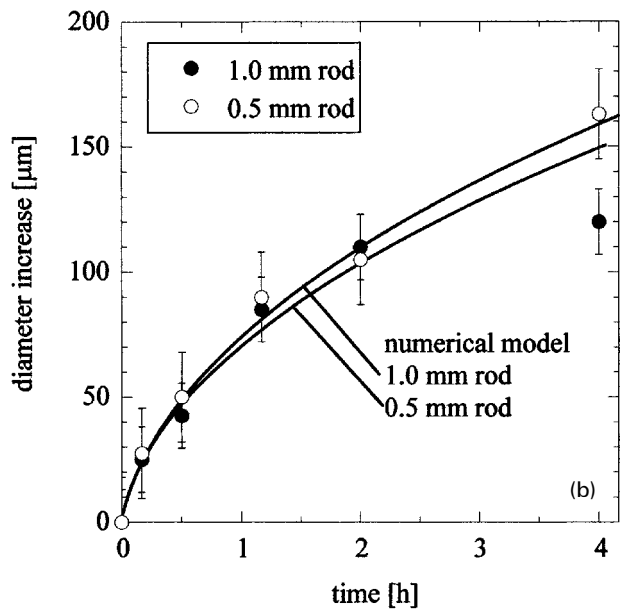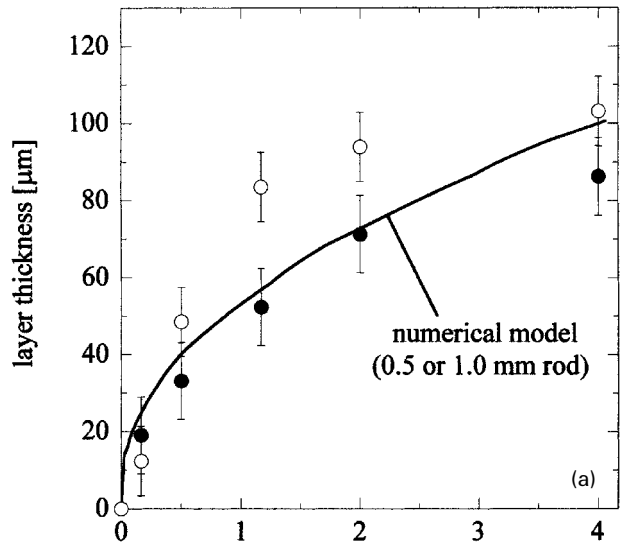
a thickness of outer Ni_2Al_3 shell; b rod diameter increase

5 Thickness of outer Ni_2Al_3 shell and rod diameter increase as functions of aluminising time for 0·5 and 1 mm rods: curves show model predictions

Numerical model

The process of aluminisation involves the interdiffusion of aluminium and nickel through a series of phases at 1000°C, i.e. Ni, Ni_3Al, NiAl, and Ni_2Al_3. In each phase, the aluminium concentration c evolves according to Fick's second law

$$\frac{\partial c}{\partial t} = \nabla \cdot (\tilde{D} \cdot \nabla c) \qquad \qquad \qquad (1)$$

where t is time and $\tilde{D}$ is the Ni – Al interdiffusion coefficient in the phase of interest, and may be concentration dependent (Kirkendall porosity is neglected). As with any multiphase diffusion problem, concentrations within any two phase field are prohibited by the phase diagram. Thus, during aluminising, the phase layers remain separated by discontinuities in concentration, and a condition of mass balance holds at each interphase boundary. Written below in a unidimensional form, assuming equal partial molar
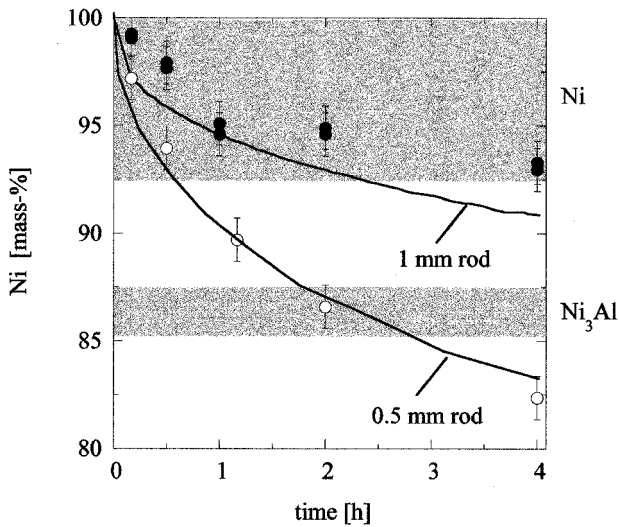
6   Time dependence of average nickel composition upon aluminisation for 0·5 and 1 mm diameter rods:[5] composition ranges of Ni, Ni₃Al, and NiAl phases at 1000°C (Ref. 11) are shown as shaded bands and theoretical predictions as continuous curves

volumes for aluminium and nickel, the mass balance gives the rate of interface s migration $\partial s/\partial t$ as

$$\frac{\partial s}{\partial t} = \frac{J_1 - J_2}{c_1^s - c_2^s}\bigg|_{x=s} \qquad \cdots \cdots \cdots \cdots \quad (2)$$

where J_p is the flux in phase p ($=1$ or 2) given by Fick's first law, x is the spatial coordinate, and c^s is the composition at the interface given by the equilibrium phase diagram. In the aluminisation process considered here, a Ni_2Al_3 layer develops at the gas/solid interface, which is subject to a constant composition $c^{s_0} = 59·6$ at.-%Al, as described above. The mass balance condition for the specimen surface is

$$\frac{\partial s_0}{\partial t} = \frac{-J_{Ni_2Al_3}}{1 - c^{s_0}}\bigg|_{x=s_0} \qquad \cdots \cdots \cdots \cdots \quad (3)$$

In the present work, a fixed grid, explicit, finite difference formulation has been used to solve equation (1), subject to the constraints of equations (2) and (3), for all four phases present during aluminisation of nickel at 1000°C. The model tracks explicitly the several moving phase fronts and the specimen surface, which are free to traverse between the grid points used in the finite difference calculations. At positions near a phase boundary, the even spacing of the grid is thus disturbed; a Lagrangian interpolation scheme is used to approximate the spatial derivatives near interfaces. The details of the general numerical method are available elsewhere,[12] in which only two phases were considered. The present analysis expands on the above work by including multiple phase boundaries, and by considering concentration dependent diffusivities.

The process of aluminisation, under conditions very similar to those considered in the present work, has previously been modelled by Hickl and Heckel,[8] who used a movable grid finite difference method. They treated the diffusivities in each phase as concentration independent, and varied their numerical values to match experimental data. Also, to model the experiments accurately, they introduced an incubation time during which no aluminisation occurred. A method similar to that of Hickl and Heckel has recently been used by Tsuji[13] to treat finite and semi-infinite diffusion couples. He considered specifically the interdiffusion reaction during aluminisation of a semi-infinite sheet of nickel, and found good agreement with the
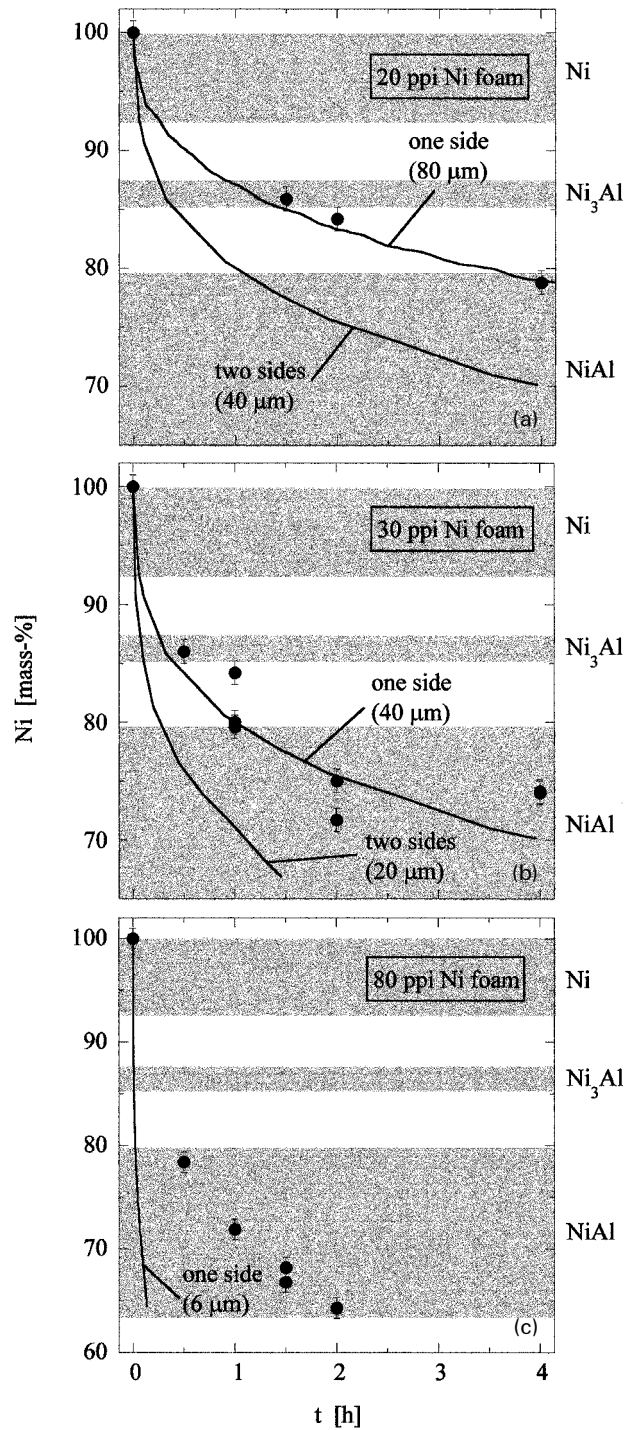

a 20 ppi; b 30 ppi; c 80 ppi

7   Time t dependence of average nickel composition upon aluminisation for foams with given pore sizes (some of these data are already reported elsewhere[5]): composition ranges of Ni, Ni₃Al, and NiAl phases at 1000°C (Ref. 11) are shown as shaded bands, and bounds for theoretical predictions as continuous curves for diffusion from one side (gas outside hollow struts) and two sides (gas inside and outside hollow struts)

experimental and theoretical results of the above authors; however, Tsuji also assumed concentration independent diffusivities, and used the fitted values obtained by Hickl and Heckel.[8]

In the present work, a different numerical method has been used to simulate the same physical process, and two major changes to the original approach of Hickl and Heckel have been implemented.[8]
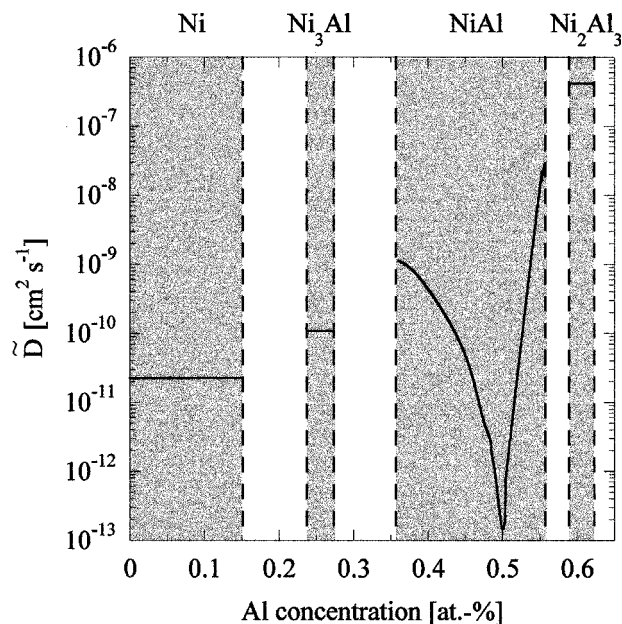
8 Composition dependence of Ni–Al interdiffusion coefficient $\tilde{D}$ in all phases present during aluminisation at 1000°C (Ref. 11 and 14)

First, because the interdiffusion coefficient varies broadly (over five orders of magnitude, Fig. 8) across the composition range of NiAl at 1000°C, it is inappropriate to assume concentration independent diffusivity. Instead, literature data have been used for $\tilde{D}$ as a function of composition in each of the phases.[11,14] As shown in Fig. 8, only NiAl exhibits significant variation.

Second, the present work is concerned with complete conversion of the metallic nickel phase to a series of intermetallic nickel aluminide phases, in contrast with the work of Hickl and Heckel[8] that considered only growth of thin surface layers. The present work is specifically interested in narrow rods aluminised from the surface, or thin sheets aluminised from one or both sides, for which the assumption of an infinite linear medium is inappropriate. A cylindrical model geometry and a linear thin sheet geometry have been used to simulate the aluminisation of rods or open cell foam strut walls, respectively. In addition to the first boundary condition of constant aluminium surface concentration, a second boundary condition requires that the flux is zero at the other surface (for diffusion from one side of the sheet) or in the specimen centre plane (for diffusion from both sides of the sheet).

An iterative scheme has been used to solve equation (1), subject to equations (2) and (3), with the concentrations at the phase boundaries as shown in Fig. 8. Details for applying the fixed grid numerical method to these geometries are given elsewhere.[12] Garcia et al.[15] have also recently considered the interdiffusion reaction of Ni–Al thin films, using a new numerical approach in which the two phase concentration fields are considered as legitimate phases in the problem, but are assigned very small diffusivities so that they attain no significant width. Although this method is more easily implemented than the one used in the present work, it requires a finite difference grid spacing of the order of an interatomic distance, as well as extremely small time steps. Their model is therefore best applied to nanoscale diffusional reactions; for the cylinders and foams considered in the present work, it would require computational power higher by about six orders of magnitude than the method used here.

Simulations were carried out for rods with diameters of 0·5 and 1·0 mm (two-dimensional cylindrical geometry, comparable to rod diffusion data) and for sheets with thicknesses of 80, 40, 20, and 6 μm (one-dimensional thin sheet geometry, comparable to 20, 30, and 80 ppi foams with strut wall thicknesses of the above dimensions, *see* Table 1). The model was used to predict the composition profiles and thicknesses of the various intermetallic layers. The average specimen composition $\bar{c}$ was also found by numerically integrating the concentration over the specimen volume as

$$\bar{c} = \frac{1}{a} \int_0^a c \, dx \quad . \quad . \quad . \quad . \quad . \quad . \quad . \quad . \quad . \quad . \quad (4a)$$

for the thin sheet geometry with thickness a, or

$$\bar{c} = \frac{2}{a^2} \int_0^a cx \, dx \quad . \quad . \quad . \quad . \quad . \quad . \quad . \quad . \quad . \quad (4b)$$

for the cylindrical geometry with radius a.

Discussion

As reported earlier,[5] vacuum annealing of the 80 ppi foams at 1000°C led to a single phase NiAl foam by homogenisation of the concentration gradients present in the struts at the end of the aluminisation step. However, the coarser 20 ppi foams, with average Ni_3Al composition, exhibited variations in composition owing to large local variations in strut wall thickness, leading to nickel poor ($NiAl-Ni_3Al$) or nickel rich ($Ni-Ni_3Al$) two phase regions. The aluminisation time and temperature affect the composition of the final intermetallic foam, unlike homogenisation, where excess annealing times and temperatures are unimportant. Thus, the model is applied here only to the first critical step of the process, i.e. the pack aluminisation step, which dictates the final composition of the foams and produces composition gradients between the surface and the centre of the specimens (rods or strut walls). The model is, however, capable of describing the subsequent homogenisation step under conditions of zero surface flux, as also carried out by Hickl and Heckel.[8]

RODS

When the model was applied to the aluminisation of cylindrical rods, the outermost intermetallic Ni_2Al_3 shell was found to grow at a very rapid rate, compared with the growth of either the NiAl or the Ni_3Al shell, as a consequence of the much higher diffusivity for the former phase (Fig. 8). In fact, at any time during the simulation, the Ni_2Al_3 shell was found to be much thicker than either of the other two shells (by a factor of 5–20, in all cases). This prediction agrees with experimental results in the present study (Fig. 3) and in a previous investigation:[5] the intermediate NiAl and Ni_3Al layers in the rods were too small to be resolved by optical metallography, while the outer Ni_2Al_3 shell was always much larger. Hickl and Heckel[8] also observed similar relative layer thicknesses in their experimental study of aluminisation of large nickel substrates at 1000°C. These authors also noted that, because of its very small thickness, the Ni_3Al layer could essentially be neglected in their numerical simulations.

The present work also included computation trials in which one or both of the NiAl and Ni_3Al layers were not included. For all of these trials, growth of the Ni_2Al_3 layer was identical, and the global composition predicted by the model was unchanged within the numerical accuracy of the method. Thus, neglecting the presence of the very thin NiAl and Ni_3Al layers produced no significant changes in the

model output. However, this simplification substantially reduces the computational complexity, as it requires the tracking of only two interfaces (i.e. the Ni_2Al_3/Ni interface and the specimen surface), and allows larger finite time steps (as given by the numerical stability criterion[12]). Furthermore, diffusion in the remaining two phases (nickel and Ni_2Al_3) can be considered to be concentration independent with reasonable accuracy (as seen in Fig. 8), which reduces the number of spatial derivatives to be computed in solving equation (1). In the following, all of the model predictions use this simplification, although concentration dependent diffusivities have still been employed.

Figure 4 shows that the measured concentration profile in rods is well described by the model, which uses no adjustable parameters. A very shallow concentration gradient exists in the Ni_2Al_3 shell, as expected from the large shell thickness and the small concentration range of that phase. Three data points are in the nominal concentration range of the NiAl shell, which exhibits a very steep concentration gradient, owing to the shell thinness and the large solubility of NiAl for both nickel and aluminium. The spatial resolution ($\sim 10 \mu m$) is insufficient to resolve unambiguously the adjacent Ni_3Al layer. Finally, the aluminum concentration profile in the nickel phase decays rapidly to non-measurable values (over $\sim 30 \mu m$), again in good agreement with the predicted profile.

Figure 5a shows that there is reasonable agreement between measurement and prediction for the evolution of the Ni_2Al_3 shell thickness in rods. At early times, the shell growth follows parabolic kinetics for diffusion into a semi-infinite body. As seen in Fig. 5b, the model also predicts the measured increase in rod diameter within experimental error, except for a single data point. The divergence of the two predicted lines after ~ 1 h is due to the effect of the finite size of the rods upon the diffusion profile. However, motion of the Ni_2Al_3/Ni phase boundary is such that the Ni_2Al_3 layer thickness is numerically identical for both rod diameters up to ~ 4 h (Fig. 5a). Finally, Fig. 6 shows that the model predicts the average concentration of both rods satisfactorily.

FOAMS

The aluminisation diffusion problem is much more complex for open cell foams than for simple cylindrical rods. First, the total specimen area is much larger for the foam, so the equilibrium surface concentration may not be maintained everywhere in the specimen. This is confirmed by the macroscopic concentration gradient observed between struts at the surface and those at the core regions of the foam specimens. Second, aluminium diffusion occurs from both outside and inside surfaces of the hollow struts, as illustrated in Fig. 2. However, the gas flux at the inner strut surface is reduced, as demonstrated by the thinner Ni_2Al_3 shell at the inner strut surface (Fig. 2), most probably because of the small number of inlets into the hollow struts. Third, the struts exhibit varying wall thickness, uneven shape, and complex junctions at the cell edges (Fig. 1), thus rendering the diffusion geometry very complex. The following simplifications are made to apply the above model to the foams: (a) the surface concentration is assumed to be constant at its equilibrium value of $c^{s_0} = 59.6$ at.-%Al at all times; (b) strut junctions are ignored; and (c) the strut walls are modelled as thin sheets with uniform wall thickness given by the average value in Table 1. Because the ratio of strut diameter/wall thickness is large, wall curvature can be ignored, and the hollow struts can be described as thin sheets that are aluminised from one or both sides.

Figure 7 shows model predictions for aluminisation occurring outside the hollow struts only (lower bound) or

both inside and outside the struts (upper bound). Experimental data are close to the lower bound for 20 ppi foams (Fig. 7a), indicating that the accelerating effect of diffusion from the strut inner surface is nearly cancelled by the decelerating effect of macroscopic concentration gradients between foam specimen surface and core. For 30 ppi foams (Fig. 7b), a few data points show kinetics slower than the lower bound, indicating that the latter effect outweighs the former. This trend is confirmed by results for the 80 ppi foam (Fig. 7c), where the observed aluminisation kinetics is much slower than predicted. For constant pack conditions, macroscopic concentration gradients (i.e. from strut to strut within the foam) should increase with increasing foam specific area. Assuming that the foam comprises uniform cylindrical struts, simple geometry shows that the foam's specific area scales directly with strut wall thickness, and inversely with foam relative density. The calculated specific area of the 80 ppi foam is then 19 times that of the 20 ppi foams, and eight times that of the 30 ppi foams. The large increase in specific area for the 80 ppi foam, which exacerbates the macroscopic concentration gradients within the foam, is thus the most likely reason for the discrepancy between predicted and observed aluminisation kinetics in Fig. 7c. Macroscopic concentration gradients within the foam could be avoided with a larger pack volume, thinner specimens, and increased gas convection (for example by using forced gas circulation). Then, fine structure 80 ppi foams could be aluminised to an average NiAl composition in very short times (less than 10 min, Fig. 7c).

In summary, the present model allows for accurate prediction of the process variables (time, temperature, and surface concentration) necessary to achieve a target composition (for example, NiAl or Ni_3Al) upon equilibrium pack aluminisation of nickel foams with known geometric parameters. After homogenisation, lightweight, single phase aluminide foams can be produced, with possible applications in the aerospace field.[5] The model also points to possible process improvements (such as increased convection when equilibrium conditions are not met).

Conclusions

A multiphase diffusion model has been developed to predict the time evolution of concentration profiles upon the aluminisation of nickel, under conditions of constant surface concentration encountered during pack aluminisation.

1. Of the three intermetallics stable at 1000°C (Ni_3Al, NiAl, and Ni_2Al_3), only Ni_2Al_3 is predicted to be present in significant amounts, as also observed experimentally. The model can thus be simplified to the case of the growth of a Ni_2Al_3 layer into a nickel phase, both phases having solid solubility for aluminium.

2. For nickel rods with 0.5 and 1 mm diameter aluminised at 1000°C for up to 4 h, good agreement is found between experimental results and model predictions for the growth of the outer Ni_2Al_3 shell as well as the concomitant increase in rod diameter and average rod aluminium composition. A calculated diffusion profile is also in good agreement with measurement.

3. The predicted evolution of the average aluminium composition agrees reasonably well with values measured on two, large cell, nickel foams consisting of open cells comprising hollow struts with wall thickness 84 and 41 μm, respectively. The predicted aluminisation kinetics for a small cell nickel foam with 6 μm strut wall thickness is, however, much faster than observed. This discrepancy can be explained by the high surface area of the last foam, which prevents the establishment of equilibrium aluminium surface concentration within the centre of the specimen.

Acknowledgements

References

1. M. F. ASHBY, A. EVANS, N. A. FLECK, L. J. GIBSON, J. W. HUTCHINSON, and H. N. G. WADLEY: ''Metal foams: a design guide''; 2000, Boston, MA, Butterworth-Heinemann.
2. D. B. MIRACLE: *Acta Metall. Mater.*, 1993, **41**, 649 – 684.
3. R. D. NOEBE, R. R. BOWMAN, and M. V. NATHAL: *Int. Mater. Rev.*, 1993, **38**, 193 – 232.
4. R. D. NOEBE, R. R. BOWMAN, and M. V. NATHAL: in ''Physical metallurgy and processing of intermetallic compounds'', (ed. N. S. Stoloff and V. K. Sikka), 212 – 296; 1996, New York, Chapman & Hall.
5. A. HODGE and D. C. DUNAND: *Intermetallics*, 2001, **9**, 581 – 589.
6. L. S. CASTLEMAN and L. L. SEIGLE: *Trans. AIME*, 1958, **212**, 589 – 596.
7. S. R. LEVINE and R. M. CAVES: *J. Electrochem. Soc.*, 1974, **121**, 1051 – 1064.
8. A. J. HICKL and R. W. HECKEL: *Metall. Trans. A*, 1975, **6A**, 431 – 440.
9. D. K. DAS, V. SINGH, and S. V. JOSHI: *Metall. Mater. Trans. A*, 1998, **29A**, 2173 – 2188.
10. D. C. DUNAND: *J. Mater. Sci.*, 1994, **29**, 4056 – 4060.
11. S. SHANKAR and L. L. SEIGLE: *Metall. Trans. A*, 1978, **9A**, 1467 – 1476.
12. C. SCHUH: *Metall. Mater. Trans. A*, 2000, **31A**, 2411 – 2421.
13. S. TSUJI: *Metall. Mater. Trans. A*, 2001, **32A**, 681 – 690.
14. S. KIM and Y. A. CHANG: *Metall. Mater. Trans. A*, 2000, **31A**, 1519 – 1524.
15. V. H. GARCIA, P. M. MORS, and C. SCHERER: *Acta Mater.*, 2000, **48**, 1201 – 1206.